# Radical Anions of Mono- and Bis-fulleropyrrolidines: An EPR Study

**Marina Brustolon,*,§ Alfonso Zoleo,§ Giancarlo Agostini,‡ and Michele Maggini†**

*Dipartimento di Chimica Fisica, Via Loredan 2, I-35131, Padova, Italy, Centro di Studi sugli Stati Molecolari Radicalici ed Eccitati del CNR, Padova, Italy, and Centro Meccanismi Reazioni Organiche—CNR, Dipartimento di Chimica Organica, Via Marzolo 1, I-35131, Padova, Italy*

*Received: March 5, 1998; In Final Form: May 13, 1998*

The radical anions of three $C_{60}$ derivatives (*N*-methyl-3,4-fulleropyrrolidine, *N*-methyl-2-(3,6,9-trioxadecyl)-3,4-fulleropyrrolidine, and bis-*N*-methyl-3,4-fulleropyrrolidine are respectively $MFP^-$, $tegMFP^-$, and $bisMFP^-$) have been investigated by continuous wave (cw) and pulsed EPR in methyltetrahydrofuran and tetrahydrofuran solutions. The EPR spectra for $MFP^-$ and $tegMFP^-$ show a 1:1:1 triplet, due to the hyperfine coupling with the pyrrolidine nitrogen. The EPR spectrum of $bisMFP^-$ shows a superimposition of two signals, each due to a 1:2:3:2:1 quintet. Each quintet is due to the hyperfine coupling with the two pyrrolidine nitrogen atoms. The two signals are attributed to two different conformers of the radical. A direct transfer of spin density from the $C_{60}^-$ sphere to the nitrogen atoms is discussed as arising from the bent conformation of the pyrrolidine rings. All the spectra show several weaker satellite lines, due to the radical anions containing a $^{13}C$ atom. From their analysis a $C_{2v}$ symmetry for the spin distribution is obtained in the case of $MFP^-$ and $tegMFP^-$. The EPR line widths of these latter radicals at room temperature are larger than those expected on the basis of spin relaxation due to rotational diffusion in solution, and the line widths decrease upon decreasing the temperature. Pulsed EPR measurements of $T_1$ in liquid and frozen solutions show that the EPR line widths are determined by the anomalously short lifetimes of the spin states. The temperature dependence of $T_1$ obeys to the Arrhenius law, giving an activation energy of 7 kJ/mol. The latter results are compared with those obtained in the past for the lone $C_{60}^-$. They are attributed to the closeness of the electronic levels, due to the weak perturbation of the pyrrolidine ring on the symmetrical electronic distribution of $C_{60}$. On the other hand, the spin relaxation properties of $bisMFP^-$ are shown those expected for a nonsymmetrical radical. The comparison of cw- and pulsed-EPR spectra of $MFP^-$ in frozen solutions of MeTHF and THF indicates the presence of aggregates of interacting radicals in THF.

## Introduction

The paramagnetic species produced by reduction of $C_{60}$ and some of its derivatives have been extensively studied with EPR in the past six years.[1−7] The attribution of the EPR signals to the different paramagnetic species is in general complicated for these systems by several peculiar features of their spectra. In many cases a hyperfine pattern is absent, and the *g* factor and the line widths are the only parameters that can be measured by cw-EPR. The high symmetry of the spin distribution can give rise to anomalously large line widths.[8,9] The fullerenes form easily aggregates, whose structure is not known. There are clear evidences that the multiple EPR signals detected can be attributed to different aggregates, whose nature and interconversion dynamics depend on solvent, concentration, and temperature.[10] Moreover, the multistage reduction is very easy, and the spin multiplicity of some of the multireduction products is still discussed.[11] As a consequence, many questions on the nature and behavior of such species are yet not completely answered.

An interesting class of fullerene derivatives is that of the fulleropyrrolidines, prepared by 1,3-dipolar cycloaddition of azomethine ylides to $C_{60}$.[12] This methodology provides a broad variety of useful functionalized fullerenes, produced with practical applications as the scope.[13] In particular, elucidation of the electronic structure of reduced fulleropyrrolidines becomes important as these compounds are extensively used as electron-accepting units in electro- and photoactive dyads.[14]

Sun et al. reported an EPR study on the radical anion of the *N*-methylfulleropyrrolidine, **1**, (Chart 1) in benzonitrile.[15] They detected a single line lacking of any hyperfine coupling. On the other hand, in a preliminary study on the same radical anion in THF, we obtained an EPR spectrum showing for $T < 240$ K a hyperfine coupling with the pyrrolidine nitrogen. Moreover, a pattern of satellite lines due to the radicals containing a $^{13}C$ isotope were observed at the wings of the main spectrum. The temperature dependence of the EPR line width was found to be anomalous with respect to the general trend of organic radicals in solution.[16]

This paper reports a continuous wave and pulsed-EPR investigation on the radical anions of *N*-methylfulleropyrrolidine, **1**, *N*-methyl-2-(3,6,9-trioxadecyl)-3,4-fulleropyrrolidine, **2**, and bis-*N*-methyl-3,4-fulleropyrrolidine, **3**, in which the second pyrrolidine ring is fused to the equatorial 6,6 ring junction of $C_{60}$ (Chart 1).

The presence of the hyperfine pattern in the EPR spectra of these radical anions makes their study particularly convenient to elucidate important features regarding symmetry and spin distribution on the fullerene spheroid.

§ Dipartimento di Chimica Fisica.
‡ Centro di sugli Stati Molecolari Radicalici ed Eccitati del CNR.
† Centro Meccanismi Reazioni Organiche—CNR.

S1089-5639(98)01385-1 CCC: $15.00 
Published on Web 07/15/1998

**CHART 1**

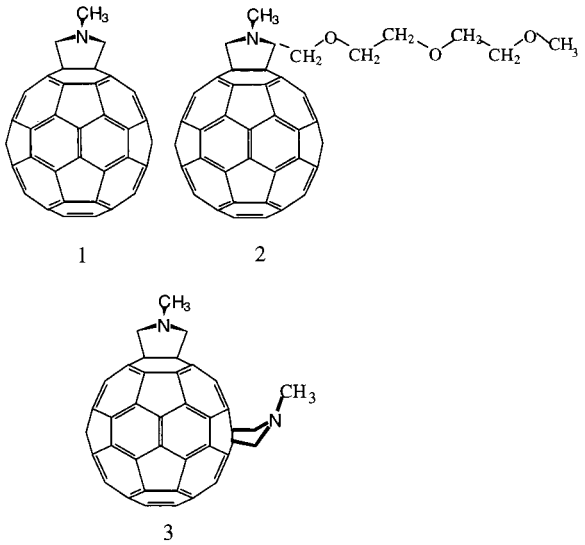

A pulsed-EPR investigation was also performed in order to throw some light on the spin relaxation properties of these systems.

## Experimental Section

**Instrumentation.** EPR measurements were performed with a computer controlled Bruker ER 200 D X-band EPR spectrometer, equipped with a nitrogen flow-temperature controller. To calibrate *g* values, the microwave frequency was measured with a 5342A Hewlett-Packard microwave frequency counter, and a LiTCNQ crystal was used as *g* value standard. The pulsed-EPR experiments were performed in the 130−300 K temperature range by using a Bruker ESP 380 spectrometer equipped with a dielectric Bruker cavity and a variable temperature unit. Vis−NIR absorption spectra were taken on a Perkin-Elmer Lambda 6 spectrophotometer.

**Materials.** Functionalized fullerenes considered in this paper are shown in Chart 1. All compounds are 3,4-fulleropyrrolidines, prepared by the reaction of the appropriate azomethine ylide precursor with $C_{60}$.[12] Derivatives **1** and **2** are products of monoaddition across a 6,6 ring junction of $C_{60}$, while compound **3** is a bis-adduct in which the second pyrrolidine ring is fused to the equatorial 6,6 ring junction of $C_{60}$. *N*-Methyl-3,4-fulleropyrrolidine, **1**,[12] *N*-methyl-2-(3,6,9-trioxadecyl)-3,4-fulleropyrrolidine, **2**,[17] and bis-*N*-methyl-3,4-fulleropyrolidine derivative, **3**,[18] were prepared and purified as described in the literature. Dibenzo-18-crown-6 was used as purchased from Aldrich. Tetrahydrofuran and methyltetrahydrofuran were distilled from sodium prior to use.

**Abbreviations Used.** The following abbreviations were used: MFP, *N*-methyl-3,4-fulleropyrrolidine; tegMFP, *N*-methyl-2-(3,6,9-trioxadecyl)-3,4-fulleropyrrolidine; bisMFP, bis-*N*-methyl-3,4-fulleropyrolidine; THF, tetrahydrofuran; and MeTHF, 2-methyltetrahydrofuran.

**Anion Preparation: General Procedure.** The radical anions of MFP, tegMFP, and bisMFP were prepared by standard vacuum ($10^{-4}$ mbar) techniques in a 10 mm o.d. Pyrex tube. The tube was equipped with three lateral arms. The first one contained the fullerene sample, in some cases together with the dibenzo-18-crown-6 ether. In the second one, a sodium mirror was formed by evaporating the pure metal from a sodium filled Drummond calibrated capillary, before introducing the solvent through the vacuum line. The third arm was equipped with a usual EPR tube and a quartz cell (path length 2 mm) for vis−NIR absorption measurements. For each anion preparation (vide infra), an aliquot of solution was introduced in the quartz cell to check the absorption features of the prepared radical. The concentrations of the compounds were $10^{-5}$ M.

**MFP, tegMFP, and bisMFP Anion Preparation.** Two methods were employed for the preparation of the radical anion of MFP, **1**. A weighted amount of MFP was dissolved in THF (or MeTHF) and brought into contact with a mirror of sodium in equimolar amount. The exact quantity of sodium to be used was taken from a sodium filled Drummond capillary (method 1). An equimolar amount of MFP and dibenzo-18-crown-6 was dissolved in THF (or MeTHF) and treated with excess sodium. The salt of the MFP monoanion was then isolated by filtration upon addition of *n*-hexane (method 2). It has been shown that dibenzo-18-crown-6 in the latter procedure prevents MFP overreduction.[11] Monoanions of tegMFP, **2,** and bisMFP, **3**, were prepared by method 2.

## Results

**Vis−NIR Absorption Spectra.** Vis−NIR absorption spectra were recorded at room temperature for the samples of MFP reduced with the two methods described above. They are shown in Figure 1.

In Figure 1a,b, the spectra obtained respectively with methods 1 and 2 are reported. The two spectra are very similar, and they are similar to the spectrum reported for $MFP^-$ by Sun et al.[15] On the other hand the spectrum reported in Figure 1c corresponds to a sample obtained with method 1, in which the ratio Na:MFP was 2:1. A comparison with the vis−NIR spectra of $C_{60}^{2-}$ shows a quite close similarity,[19] with a blue shift of ca. 70 nm of the NIR band for $MFP^{2-}$. These spectra, together with the EPR results, indicate that the reduction of MFP with sodium can be controlled and stopped to the production of the monoanion by using method 1 or 2.

**Cw-EPR Spectra of $MFP^-$.** The cw-EPR spectra of $MFP^-$ in liquid solutions of THF and MeTHF are very similar. At room temperature, the spectrum shows a single line with a width of 0.7 G, which sharpens by lowering the temperature. At $T =$ 240 K a 1:1:1 triplet appears, which becomes more evident at still lower temperature due to a further sharpening of the lines. Spectra at 240 and 225 K are reported in Figure 2a, and at 190 K in Figure 4.

The simulation of the spectra in liquid solution shows a hyperfine coupling constant $a = 0.22$ G, which is temperature independent, whereas the line width varies with the temperature: Figure 3 shows the $1/T_2$ values as function of the temperature (as known $1/T_2\ [s^{-1}] = 1.52 \times 10^7\ \Delta H_{pp}$ [G], where $\Delta H_{pp}$ is the peak-to-peak line width).

The line widths are the same in THF and MeTHF liquid solutions in the temperature range where the line widths decrease on decreasing the temperature, becoming slightly different at the lowest temperatures (140 K < $T$ <180 K: at 160 K, $\Delta H_{pp}=$ 0.11 G in THF and 0.08 G in MeTHF).

For $T$ < 220 K, weaker satellite lines due to radicals containing a $^{13}C$ nucleus can be seen in the wings of the main spectrum, repeating the same triplet pattern. The satellite lines were simulated on the basis of a best fit procedure on varying the number of different $^{13}C$ hyperfine couplings, the relative abundances of the radicals bearing each type of coupled $^{13}C$ nucleus, and the values of the hyperfine coupling constants. The initial parameter set was obtained by assuming a spin density distribution similar to that calculated for the $C_{60}$ monoanion by Koga et al.[20] They obtained a spin distribution with maxima

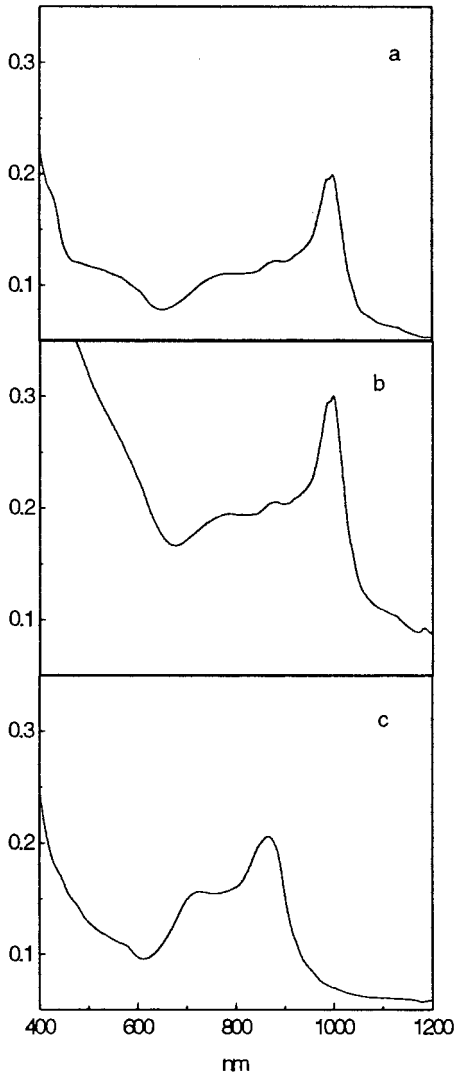


**Figure 1.** Absorption spectra in the near-infrared of *N*-methylfulleropyrrolidine reduced in tetrahydrofuran. (a) Radical anion obtained from the reduction with an equimolar quantity of sodium (method 1, see text). (b) Radical anion obtained with an equimolar amount of the fulleropyrrolidine and crown ether dibenzo-18-crown-6 and an excess of Na (method 2). (c) Radical dianion obtained from the reduction with a ratio Na:MFP 2:1.

on carbon atoms 5 and 8, see Chart 2. Arena et al. obtained an approximate spin density distribution for the radical anion of MFP by calculating the LUMO coefficients of the neutral molecule,[21] and the results are again that the maxima of the spin density are on the equatorial belt of the fullerene sphere, positions 5,5′ and 8,8′ in Chart 2 ($\rho \approx 0.05$ on each carbon atom). An initial set of hyperfine couplings was obtained by using the well-known Fraenkel−Karplus semiempirical relationship, based on the spin polarization effects of the C−C bonds in a planar radical.[22] This relationship is slightly incorrect for the nonplanar $MFP^-$ radical, but it gives a reasonable initial parameter set.

The best agreement was obtained by assuming that the pattern was originated by four groups of nonequivalent carbon atoms each comprising, respectively, 2, 2, 4, and 4 equivalent carbon atoms, with the hyperfine couplings reported in Table 1. The spectrum simulated on the basis of these assumption is reported in Figure 4.

The *g* factor was measured and a temperature independent value of 1.9999 was obtained in both solvents. We studied also the spectrum of $MFP^-$ in frozen THF and MeTHF solutions ($T$ = 130 K). The line width increases in both solvents from the liquid to the frozen solutions, giving rise to an EPR signal in which the hyperfine pattern due to $^{14}N$ is not detectable. However, whereas the spectrum in MeTHF can be simulated by a Lorentzian line 0.9 G wide, the spectrum in THF appears more complex (see Figure 5). In this figure we report the cw-EPR spectrum and its simulation. In the inset we report the central part of the continuous wave spectrum and the echo-detected EPR spectrum for comparison. The two peaks indicated by the arrows in the inset can be attributed to interacting radical pairs. The simulated spectrum reported in the same figure was obtained as a superposition of a Gaussian line with a width of 4 G, as well as a powder spectrum of a triplet with fine parameters $D = 11$ G, $E \sim 0$ G, and line width

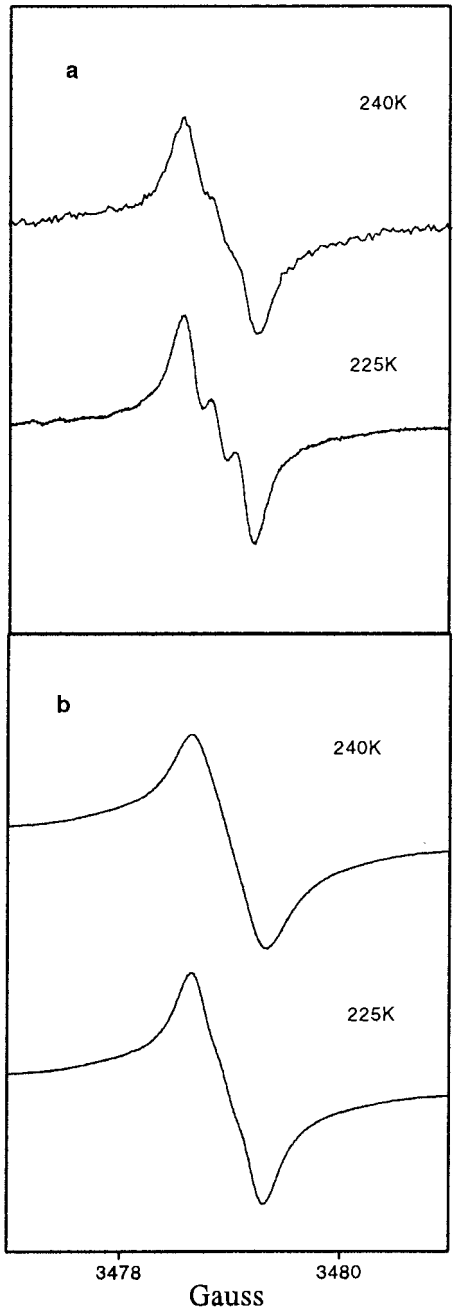


**Figure 2.** EPR spectra of $MFP^-$ (a) and $tegMFP^-$ (b) in THF at $T$ = 240 K (top) and $T$ = 225 K (frequency = 9.74 GHz; modulation amplitude = 0.05 G).

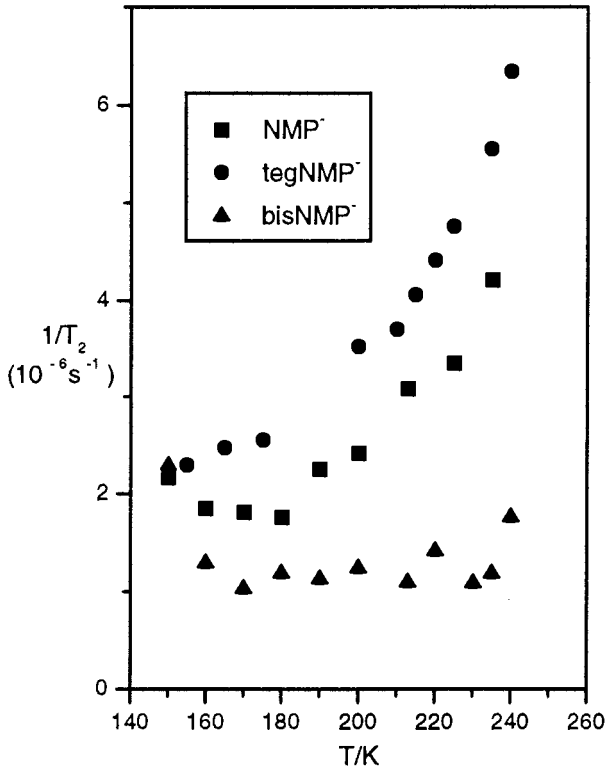


**Figure 3.** Temperature dependence of $1/T_2$ of the radical anions $MFP^-$ (circles), $tegMFP^-$ (squares), and $bisMFP^-$ (triangles) in THF solution.

**CHART 2**

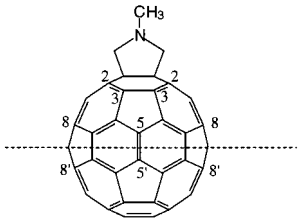

**TABLE 1: Hyperfine Coupling Constants and Number of Equivalent $^{13}C$ Atoms Obtained by the Simulation of the EPR Spectra of $MFP^-$ and $TegMFP^-$ Radicals**

| $A(^{13}C)$/G | no. equivalent $^{13}C$ |
|---|---|
| 2.07 | 2 |
| 1.63 | 2 |
| 1.19 | 4 |
| 0.75 | 4 |

4.5 G. The experimental spectrum is slightly asymmetric, probably due to the $g$ tensor anisotropy and/or a small $E$ parameter.

The echo-detected EPR spectrum will be described later.

**Cw-EPR Spectra of $tegMFP^-$.** The cw-EPR spectra of $tegMFP^-$ have been studied in THF. At room temperature, the spectrum shows a single line with a width of 0.7 G, which sharpens by lowering the temperature. At $T = 230$ K, a 1:1:1 triplet appears that can be simulated with a hyperfine coupling $a = 0.23$ G. The line widths are slightly larger than those of $MFP^-$. Also the pattern of the satellite lines due to $^{13}C$ is the same as for $MFP^-$.

Two spectra at two different temperatures are reported in Figure 2b.

**Cw-EPR spectra of $BisMFP^-$.** The EPR spectra of $bisMFP^-$ (Figure 6) at different temperatures in THF were simulated with a nonlinear best fitting program as the superposition of two

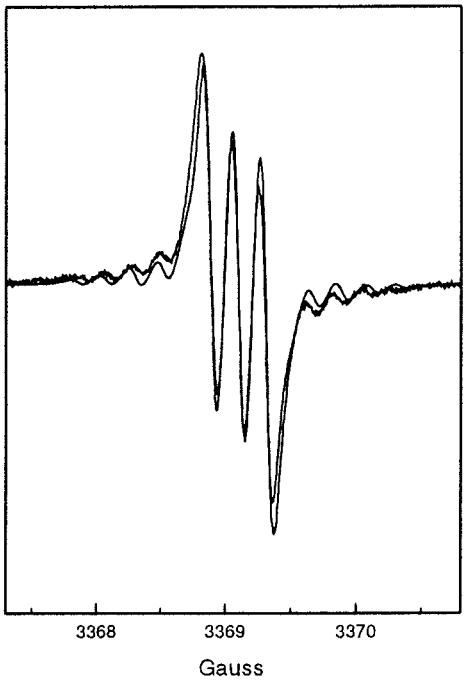


**Figure 4.** Experimental and simulated (thinner line) EPR spectrum of $MFP^-$ at $T = 190$ K (see text) in THF.

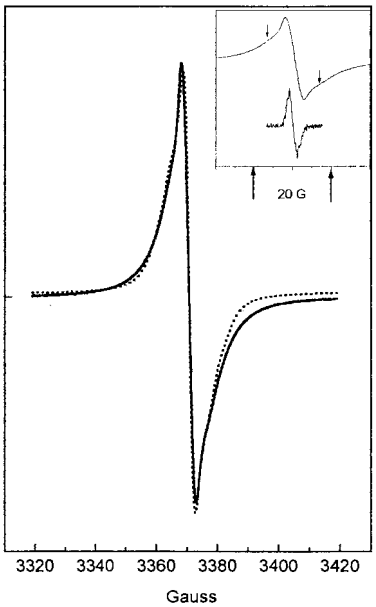


**Figure 5.** Experimental and simulated EPR spectrum of $MFP^-$ in THF frozen solution, $T = 140$ K. In the inset are reported: above the central part of the EPR spectrum, below the derivative of the corresponding echo-detected EPR spectrum (pulse widths 80 and 160 ns, separated by 320 ns).

signals, each due to a quintet 1:2:3:2:1 produced by the hyperfine coupling with two equivalent $^{14}N$ nuclei. We attribute the two signals to two slightly different radicals, hereafter termed radical 1 and radical 2. It is worth to be noted that the simulations are fairly good by assuming that the hyperfine couplings with the two nitrogen nuclei in each radical are equal, although a small inequivalence of the two $^{14}N$ hyperfine couplings for each radical cannot be ruled out.

The fitting parameters were the relative weights of the two species $w_1$ and $w_2$, their hyperfine couplings $A_1$ and $A_2$, their line widths, and the $g$ factors $g_1$ and $g_2$. At any temperature, $w_1 \approx w_2$. The average line widths for the two radicals are

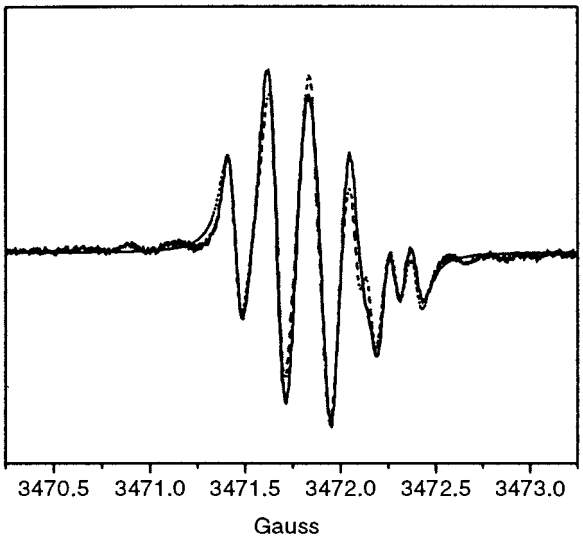


**Figure 6.** Experimental (solid line) and simulated spectra of bisMFP$^-$ at 230 K. The simulation has been performed by assuming the presence of two radical anions each showing the coupling with two equivalent $^{14}$N nuclei.

**TABLE 2: Hyperfine Coupling Constants and *g* Factors for the Two Radicals Obtained from the Reduction of BisMFP**

| *T*/K | $A_1$/G | $A_2$/G | $g_1$ | $g_2$ |
|---|---|---|---|---|
| 150 | 0.220 | 0.223 | 2.001 17 | 2.001 03 |
| 190 | 0.210 | 0.240 | 2.001 26 | 2.001 13 |
| 230 | 0.212 | 0.244 | 2.001 32 | 2.001 20 |

reported in Figure 3, together with those of MFP$^-$ and tegMFP$^-$ radicals. The results for the hyperfine coupling constants and the *g* factors for some temperatures are reported in Table 2.

Radicals 1 and 2 have slightly different $^{14}$N hyperfine couplings, but they are very similar to those of MFP$^-$ and tegMFP$^-$. The *g* factors are larger than those of the two latter radicals.

A pattern of satellite lines due to the radicals containing a $^{13}$C can be seen at the wings of the spectrum. The simulation of this pattern is complicated by the superposition of several lines. However, the two largest $^{13}$C hyperfine couplings can be measured directly from the separation of the satellite lines from the corresponding ones of the main spectrum: for radical 1, $A_C = 1.52$ G, for radical 2 $A_C = 2.34$ G. The line width varies with the temperature as reported in Figure 3.

***T*$_1$ Measurements of MFP$^-$.** We determined the $T_1$ longitudinal relaxation time for the radical both in liquid and in frozen THF solution.

In liquid solution a FID was detected. The inversion recovery of the magnetization was observed with the pulse sequence $\pi - T - \pi/2 - t$ by varying the time *T* between the inverting pulse and the $\pi/2$ pulse giving rise to the FID. The lengths of the $\pi$ and $\pi/2$ pulses were 24 and 16 ns, respectively. An exponential fit of the recovery curve gave the $T_1$ values at the different temperatures.

In frozen solution the FID becomes very short due to the presence of many spin packets with different Larmor frequencies corresponding to different anisotropic magnetic interactions. However, a refocalization of the spin packets gives rise to an echo. Therefore, $T_1$ can be measured by detecting the saturation recovery of the echo. The pulse sequence used was composed by a burst on saturating pulses of length $P_1$, followed by a sequence of two pulses giving rise to a Hahn echo after a variable evolution time *T*:

$$(P_1 - t_1)_N - T - P_0 - t_2 - P_0 - \text{acq}$$

The length of the $N = 12$ saturating pulses was $P_1 = 24$ ns, with an interval $t_1 = 400$ ns between them. The two pulses producing the Hahn echo had a length of 16 and $t_2 = 200$ ns. The relaxation time $T_1$ was obtained again with an exponential fit of the recovery curve.

In Figure 7 we report in a logarithmic plot the values $1/T_1$ against $1/T$, obtained both in liquid (circles) and in solid (triangles) solutions by the pulsed experiments. In the same plot we report also the nonsecular contribution to the cw-EPR line widths (squares) obtained as follows. The line width in the presence of lifetime broadening is given by the expression 1:[23]

$$1/T_2 = 1/T_2^0 + 1/(2T_1) \quad (1)$$

where $1/T_2^0$ is the residual line width due to secular relaxation broadening, which is proportional to the correlation time $\tau_c$ of the tumbling motion of the radical in solution. At low temperature the contribution to the line width due to $1/T_1$ is negligible, and we assumed that the line width value at $T =$ 140 K corresponds to $1/T_2^0$ at that temperature. This value was then corrected at the different temperatures. At any temperature $\tau_c$ was calculated by taking into account the viscosity of the solvents,[24] in agreement with the well known Debye expression,[23] and a temperature dependent value for $1/T_2^0$ was obtained. From relation 1 we were able to obtain the $1/T_1$ values reported in Figure 7.

As one can see the $1/T_1$ values in liquid solution obtained from cw-EPR and the inversion recovery of the magnetization lay with very good approximation on the same straight line.

The linear plot suggests that a temperature activated process affects the lifetime $\tau_s$ of the spin state, which is therefore given by the relation 2:

$$\tau_s = \tau_0 \exp(\Delta E/kT) \quad (2)$$

The best fit gives a preexponential factor $\tau_0 = 3 \times 10^{-9}$ and an activation energy $\Delta E = 7.8 \pm 0.5$ kJ/mol (652 cm$^{-1}$). From the data obtained from the saturation recovery in frozen matrix we obtain an activation energy of $6 \pm 1$ kJ/mol and a preexponential factor $\tau_0 = 36 \times 10^{-9}$.

***T*$_1$ Measurements for tegMFP$^-$.** We tried to determine the $1/T_1$ longitudinal relaxation rate for the radicals in THF liquid solution at different temperatures with an inversion recovery of the magnetization.

In liquid solution an FID was detected. For temperatures above 180 K it was impossible to invert the FID, because it recovered in a time $t < 120$ ns. For temperatures below 180 K the inverted FID was recovering so rapidly that the measurement of $T_1$ was affected by a large error.

**T$_1$ Measurements for tegMFP$^-$.** We determined the $1/T_1$ longitudinal relaxation rate for the radicals in THF liquid solution at room temperature with an inversion recovery of the magnetization.

The FID can be easily inverted at room temperature. The value obtained at $T = 290$ K is $1/T_1 = (8.0 \pm 0.5) \times 10^5$ s$^{-1}$ for both radicals.

**Echo-Detected EPR spectrum of MFP$^-$.** To gain some insight into the nature of the line broadening observed in THF frozen solution, we recorded the echo-detected EPR spectrum of MFP$^-$ at 140 K. The echo-detected EPR spectra are obtained by recording the two pulses Hahn echo amplitude as a function of the magnetic field.[25]

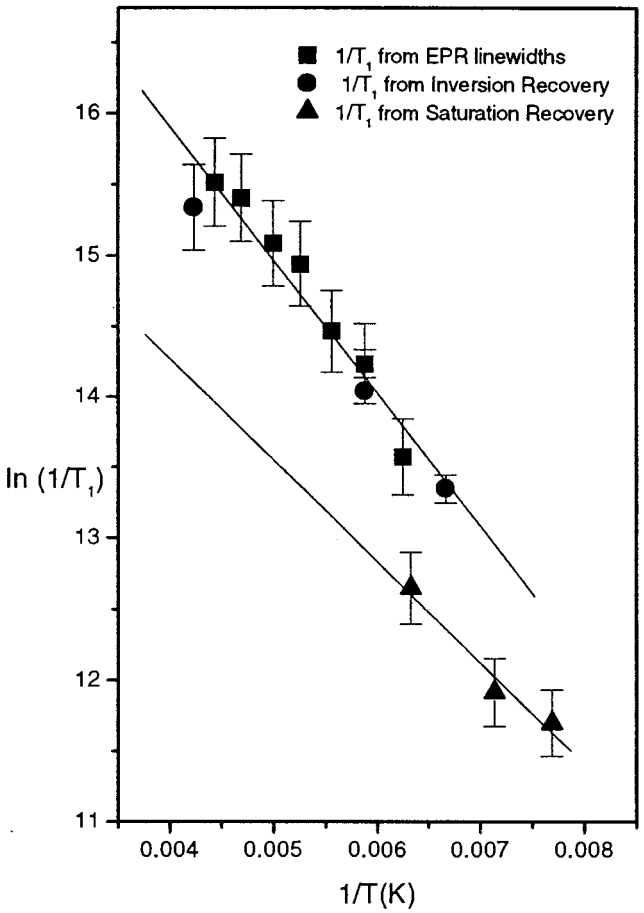


**Figure 7.** Logarithmic plots of the values $1/T_1$ ($s^{-1}$) vs $1/T$ for $MFP^-$ in THF obtained from the different EPR experiments.

When the phase memory time $T_M$ is the same for all the spin packets, the echo-detected EPR and EPR spectra give the same information. On the other hand, if more than one paramagnetic species is present with different $T_M$'s, the two types of spectra can be substantially different. In fact in the latter case in the echo-detected EPR spectrum the intensities of the lines due to the different paramagnetic species are different.

The echo-detected EPR spectrum of $MFP^-$ in frozen solution is substantially sharper than the EPR spectrum, the spin packets corresponding to the wings of the spectrum decaying with a short phase memory time $T_M$. It can be roughly simulated by a Gaussian line with a line width of 1.5 G, to be compared with the value of 4 G for the line width of the cw-EPR line, see inset in Figure 5.

## Discussion

**$MFP^-$ and tegMFP$^-$.** The similar EPR results for these two radicals indicate that the triethylene glycol substituent in position 2 of the pyrrolidine ring in $tegMFP^-$ affects only slightly the electronic properties of the molecule compared to those of parent **1**. Therefore, we will discuss these two radical anions together.

The *g* factors of the two radical anions are very similar to that of the $C_{60}^-$ radical anion. This fact indicates that their electron wave functions are not too different from those of $C_{60}^-$. In fact, the *g* factor of the $C_{60}^-$ is quite distinctive of the nearly triple degeneracy of the LUMO orbitals of $C_{60}^-$.[26]

The calculations for $C_{60}^-$ [20] showed that the Jahn−Teller distortion removes the degeneracy of the three LUMO orbitals $t_{1u}$ originating from the $I_h$ symmetry of the unperturbed $C_{60}$ molecule. Koga et al. analyzed the electronic structure of the $C_{60}^-$ on the basis of the three distorted structures of symmetry $D_{5d}$, $D_{3d}$, and $D_{2h}$. The three structures are nearly degenerate, and rearrangements between them could take place easily. The SOMO orbitals for the three structures are localized mainly around the equator and have small coefficients at the poles. Therefore we can expect that the $\pi$ electron distribution would not be much affected by the presence of the pyrrolidine group.

As explained above, the spin distribution in the $MFP^-$ was evaluated in Arena et al.[21] by taking the squares of the LUMO coefficients obtained from a restricted HF calculation on the neutral *N*-methylfulleropyrrolidine. These spin densities are considered quite reliable since it is known that the addition of a single electron to a large system changes only slightly the electron distribution. The carbon atoms bearing the largest spin densities, see carbons 5,5′ and 8,8′ in Scheme 2, were found to be in the same positions in the fullerene sphere as found in Koga et al.[20] for $C_{60}^-$. The removal of the symmetry plane indicated by the broken line gives rise to four nonequivalent sets of carbon atoms.

It should be noted that there is a quite good agreement between the calculated spin density distribution and the results of the analysis of the $^{13}C$ hyperfine pattern summarized in Table 1. The number of the different groups of carbon atoms, as well as the number of the populations of isotopically susbstituted radicals inside each group, corresponds to the number of carbon atoms 5,5′,8,8′. The expected $C_{2v}$ symmetry of the wave function is therefore experimentally confirmed. Moreover, the hyperfine couplings calculated with the Karplus−Fraenkel method and the calculated spin distribution are reasonably similar to the experimental ones.

The nitrogen hyperfine coupling constant is too large to be explained by a spin polarization of the C−C and C−N bonds. In fact the nitrogen nucleus is in $\gamma$-position with respect to the nearest carbon atoms in the fullerene moiety bearing some spin density (carbon atoms 2 in Chart 2). In very few cases in the literature one can find examples of $a_N^\gamma \neq 0$. A value $a_N^\gamma = 0.2$ *G* is reported for an uracil radical[27] where the nitrogen atom is in the $\gamma$-position with respect to the carbon atom bearing the localized unpaired electron, with $\rho_C = 1$. In the present case we know on the basis of the calculations reported above, as well as from the experimental values of the $a_{13C}$ hyperfine couplings, that the spin density is largely delocalized and is small at the poles of the sphere. The calculated spin density on carbon atoms 2 is $\rho = 0.0003$. Moreover, also the absence of any coupling with the pyrrolidine protons suggests a direct through space transfer of spin density from the distribution on the fullerene spheroid to the pyrrolidine nitrogen. In agreement with the latter considerations are also the results of a semiempirical calculation of the electronic structure of $MFP^-$ reported by Sun et al.,[15] showing a very small spin density transfer on the pyrrolidine carbon atoms.

The lowest energy conformation of the pyrrolidine rings is known to be bent. In particular for *N*-methylpyrrolidine the lowest energy conformation obtained with Hartree−Fock ab initio calculations is an envelope conformation with the nitrogen atom out of the plane of the carbon atoms with a flap angle of 45°. The CNC angles show a nearly $sp^3$ hybridization, and the orbital bearing the lone pair is in the axial position.[28] Also the restricted HF calculation on the neutral MFP gives a minimum energy conformation with the pyrrolidine ring in the envelope conformation and with the lone pair pointing toward the fullerene sphere.[21] Experimental evidence of a possible interaction between the nitrogen lone pair orbital and the fullerene $\pi$-system is given by the very low basicity of the pyrrolidine

nitrogen.[29] On the other hand, there are other examples of through space interactions between the fullerene $\pi$-system and some orbitals on the functional group. This effect has been suggested for some spiromethanofullerenes and it has been called *periconjugation*.[30] The $sp^3$ lone pair orbital of the nitrogen atom can interact with the $\pi$ distribution on carbon atoms 2 and 3 (see Chart 2). Since the calculated spin density from the LUMO orbital squared coefficients on carbon atoms 3 is $\rho_C(3) = 0.02$, 100 times larger than that on carbon atoms 2, we assume the very simple model of a spin density $\rho_N = \rho_C(3)S$, where $S$ is the overlap between the $C_3$ 2p orbitals and the $sp^3$ orbital on the nitrogen. Then the nitrogen hyperfine coupling can be obtained from the expression $A_N = A_{2s}^N 0.25\rho_N$, where $A_{2s}^N = 647$ G is the value of the hyperfine coupling for an unpaired electron in the $^{14}N$ 2s orbital[31] and 0.25 is the fraction of s-character of the $sp^3$ orbital.

The overlap calculated by assuming the pyrrolidinic ring in the envelope conformation and Slater type orbitals is $S = 0.05$, corresponding to $\rho_N = 2 \times 10^{-3}$, and therefore from the expression above $A_N = 0.3$ G, in good agreement with the observed hyperfine coupling constant (0.22 G).

Sun et al. detected a single EPR line for $MFP^-$ in benzonitrile.[15] It should be noted that, due to the very small hyperfine coupling constant of $^{14}N$, an EPR line width slightly larger than that found in THF and MeTHF in the range 240−150 K can make the three lines to overlap. A spin lattice relaxation slightly faster than that in the ethereal solvents could be the cause of a larger line width.

Radical anions of some fulleropyrrolidines were also obtained in Arena et al.[21] The derivatives studied in the latter work were characterized from a nitroxide group bonded to the pyrrolidine ring. A prolonged reduction of these species gave rise to an EPR spectrum recorded only at room temperature showing a single line with a width of 0.78 G and $g = 1.9999$. This spectrum has been attributed to a radical anion in which the unpaired electron was confined on the fullerene $\pi$-system, and the nitroxide group had been reduced. If this hypothesis is true, the radical anion would be very similar to the radical anions $MFP^-$ and $tegMFP^-$ described in the present work. The $g$ factor and the line width reported above, too large to detect the $^{14}N$ hyperfine pattern, agree well with those of the latter radicals at room temperature.

Proton and carbon NMR spectra show that the intramolecular interconversion between the two different conformers corresponding to the two possible conformations of the pyrrolidine ring is fast enough to give the equivalency of the methylene protons and carbons.[12] However, by comparing the EPR results for **1**−**3** one gets good evidence that in the EPR time scale the interconversion is slow at any temperature. In fact, for $tegMFP^-$, one expects that the interconversion energy barrier should be large, due to the steric hindrance of the triethylene glycol chain. The assumption of a slow interconversion is also in agreement with the attribution (discussed below) of the two different radicals of $BisMFP^-$ to two different isomers originating from non-interconverting bent conformations of the rings, as shown in Figure 8.

As discussed above the symmetry of the spin distribution of $MFP^-$ and $tegMFP^-$ belongs to the $C_{2v}$ group. However, the perturbation produced by the attached pyrrolidine ring on the symmetry of the $\pi$ spin distribution is weak enough to allow still anomalous spin relaxation effects. The temperature dependence of the EPR line widths, and the value of the spin lattice relaxation rate $1/T_1$ can in fact be explained only by a residual symmetry of the spin distribution. In general, the EPR line

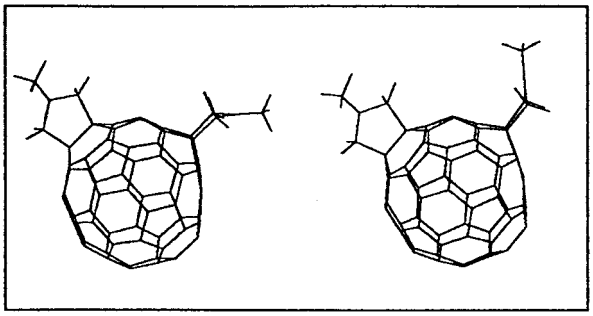

**Figure 8.** Two conformers of the molecule of bisMFP. We attribute the two overlapping EPR spectra shown in Figure 6 to the radical anions of the two conformers.

widths of radicals in dilute solutions depend only on the modulation of the Zeeman and hyperfine interactions due to the rotational diffusion. For rotational correlation times typical of medium-sized radicals in low viscosity solutions, only the secular and pseudosecular contributions to the electron spin relaxation must be taken into account in the X-band EPR spectroscopy. Therefore, in this motion régime the spin lattice time $T_1$ is longer than the spin−spin relaxation time $T_2$. The line widths are proportional to the correlation time of the motion, and therefore they increase on increasing the viscosity of the solution. Thanks to this particular relaxation mechanism, the EPR spectral profiles of many radicals have been studied to obtain information on their tumbling motions in solution or on the relative signs of their hyperfine and $g$ tensors components.[23]

On the other hand, it is well-known that the behavior of radicals of high symmetry is very different from the one described above. In fact, they give rise to EPR spectra with anomalously broad line widths, which decrease on decreasing the temperature. This behavior has been attributed to specific relaxation processes originating from the near degeneracy of the electronic energy levels.[32] A number of possible mechanisms have been proposed. They are based on the time dependent perturbations of the environment that remove the degeneracy of the electronic ground state and therefore modulate the spin−orbit coupling. These early studies have been more recently reconsidered in the light of the striking behavior of $C_{60}^-$. It gives rise to a single EPR line whose width at room-temperature varies between 40 and 80 G depending on the solvent.[33] The measurement of the electron spin $T_1$ by pulsed experiments in the range 10−40 K show an activation energy of 200−250 $cm^{-1}$, depending on the solvent.[33] Above 50 K the EPR line widths are completely determined by the fast electron spin lattice relaxation.[33] The extrapolation of the $T_1$ values to higher temperatures gives a spin lifetime of ≈1 ns at room temperature. This very short spin lifetime has been attributed to radiationless transitions between different spin states, differently affected by spin−orbit interactions. The small activation energy indicates the closeness of the energy levels involved, due to the small Jahn−Teller distortions and to the small environmental effect. A dynamic Jahn−Teller effect (pseudorotation) could be responsible for the radiationless transitions.

Recently, the attention has been drawn also to the effects on the spin relaxation of the fullerene radical anions caused by the equilibria between different aggregates in solution.[10] The tendency of fullerenes to give rise to aggregates is now well documented.[34] The differences of line widths in different solvents could be in part attributed to chemical equilibria between aggregates. However, the very short spin lattice relaxation times of $C_{60}^-$ spectra in frozen matrixes at low

**TABLE 3: Spin Lattice Relaxation Rates ($T = 290$ K)**

| | $1/T_1$ | reference |
|---|---|---|
| $C_{60}^-$ | $10^9$ s$^{-1}$ | 33 |
| MFP$^-$ | $10^7$ s$^{-1}$ | this work |
| bisMFP$^-$ | $8 \times 10^5$ s$^{-1}$ | this work |

temperatures must be explained in any case by a process involving the isolated radical anions.

In the case of the two monoderivatives studied in this paper, the EPR line widths at room temperature are only about 0.7 G, 2 orders of magnitude smaller than that of $C_{60}^-$. However, the EPR line widths decrease on lowering the temperature, showing therefore the same anomalous trend observed in $C_{60}^-$, as well as in general, in the high-symmetry radicals. The line widths are given by the sum of a secular contribution, due to the tumbling of the radicals in solution and of a nonsecular contribution due to the short lifetime of the spin state. The comparison of this latter nonsecular contribution with the spin lattice relaxation rate $1/T_1$ measured with the pulsed experiments for MFP$^-$ shows a good agreement, see Figure 7. The similar slopes of the temperature dependences of the $\ln(1/T_1)$ values in liquid and frozen solutions indicates that the spin lattice relaxation rate is determined in both environments by a process with nearly the same activation energy. Because an intramolecular interaction must be assumed as originating the spin lattice relaxation in frozen solutions, the same type of interaction must be also responsible for the spin lattice relaxation in liquid solution. On the other hand, the preexponential factor $\tau_0$ in the frozen matrix is longer than in liquid solution, as expected.

The $1/T_1$ value calculated at room temperature from the best fitting line is reported in Table 3, together with those of $C_{60}^-$ and bisMFP$^-$.

We suppose that the short lifetime of the electron spin states for $C_{60}^-$ and the fulleropyrrolidine radicals originate both from radiationless transitions between different electronic doublet states. One of these states, characterized by a particular conformation of the fullerene sphere, has a longer lifetime with respect to the other ones, and it gives rise to the detected EPR spectrum. In the case of MFP$^-$ and tegMFP$^-$, the lifetime of this state is sufficient to appreciate the differences in hyperfine couplings between the different carbon atoms. The shorter lifetime of the other state(s) give rise to EPR spectra too broad to be detected.

Other relaxation mechanisms giving rise to a fast electron spin lattice relaxation are difficult to envisage, since they should be characterized by a very fast modulation producing a large variation in a magnetic parameter of some non secular term of the spin Hamiltonian. Since the hyperfine coupling terms are absent or very small, the only parameter to consider for this role is the $g$ tensor. A modulation of the $g$ tensor due to the conformational rearrangements of the fullerene sphere could give rise to time dependent nonsecular terms of the type $g(t)S_{\pm}$. In this hypothesis, the $g$ factor would be an average value which should depend strongly on the populations of the different conformations of the radical. However, the $g$ factors measured for the $C_{60}^-$ radical anion and also for the radical anions of different derivatives in many different environments are very similar. Moreover, the relevance of the symmetry in determining the spin relaxation behavior is proved clearly by the fact that the $1/T_1$ value measured for the less symmetric radical bisMFP$^-$ is smaller than that of MFP$^-$ of an order of magnitude, see Table 3. The activation energy obtained from the logarithmic plot of $1/T_1$ vs $1/T$ for MFP$^-$ is equal to 652 cm$^{-1}$, only 2−3 times larger than in the $C_{60}^-$ case.

The temperature dependence of the line widths for tegMFP$^-$, analogous to that of MFP$^-$, indicates a similar relaxation behavior. It should be noted that in the latter case the line widths are slightly larger than for MFP$^-$. This observation indicates a larger contribution to the EPR line widths due to the lifetime broadening. In fact, the $T_1$ values were too short to measure them precisely by the inversion recovery pulsed experiment, as discussed above.

Let us now discuss the EPR spectra of MFP$^-$ in frozen solutions. The Lorentzian shape of the single line obtained in frozen solution of MeTHF can be explained by a residual mobility of the radical in the glassy solvent. The line width of 0.9 G corresponds nicely to the total line width of the EPR signal in solution taking into account a slightly increased line width due to the frozen matrix. On the other hand, in frozen THF solution the line shape is Gaussian, and the line width increases from approximately 0.1 G in liquid solution to 4 G in frozen solution. Moreover, two lateral components appear which can be simulated as belonging to a triplet with an electron−electron dipolar parameter D = 11 G, see Figure 5. Therefore we conclude that in frozen solution of THF isolated radicals, radical pairs and radical clusters are present, and the line width increase is due to an inhomogeneous broadening due to the superposition of different spectra. From the value of the $D$ parameter, by assuming the very simple model of two localized electrons with a distance of $r$ between them, from the relation 3[23]

$$D = 3g_e\beta_e/2r^3 \tag{3}$$

a value $r = 14$ Å is obtained.

The echo-detected EPR spectrum shows a narrower line (1.5 G). This narrowing is due to the very fast decay of the echoes in the wings of the inhomogeneously broadened signal. Therefore the phase memory time of the radical pairs is shorter than that of the isolated radicals. In fact the time modulation of the electron−electron dipolar interaction due to residual motions in the glassy matrix is a very efficient relaxation mechanism. The echo-detected EPR spectrum can be attributed to radicals far away enough from other radicals to have a small dipolar coupling.

The differences between the spectra in MeTHF and THF frozen solutions can be explained by the well-known fact that MeTHF forms a glass, while THF crystallizes, when the solvents are cooled. Where the solvent on freezing gives rise to microcrystals the radical anions cannot be included in the crystalline matrix and they gather together in clusters.

It should be noted that Sun et al. studied by cw-EPR the radical anion of MFP$^-$ in frozen solutions of benzonitrile (a solvent that is known to crystallize without forming glass when cooled) in the range 4−157 K.[15] They observed a single line, whose width, at 157 K, is approximately 2 G. The line width decreases on decreasing the temperature.

On the basis of the discussion above, we conclude that the EPR line broadening effect in frozen solutions of fullerenes derivatives monoanions depends strongly on the nature of the matrix, which controls the aggregation or dispersion of the radicals and their residual motions.

## Conclusions

Fulleropyrrolidine radical anions in ethereal solvents show EPR spectra with $^{14}$N and $^{13}$C hyperfine couplings. The bending of the pyrrolidine ring allows a direct mixing of the lone pair orbital on the nitrogen atom with the $\pi$ distribution on the

fullerene sphere. The $^{13}C$ hyperfine couplings are compatible with a $C_{2v}$ symmetry of the radicals of the monofunctionalized derivatives.

In the mono- and bis-functionalized $C_{60}$ derivatives, the doublet spin state giving rise to the EPR spectrum have a lifetime at room temperature of 0.1 and 1 $\mu$s, respectively. This feature shows that monofunctionalized $C_{60}$ monoanions retain still some of the properties of $C_{60}^-$ due to the high symmetry of the fullerene sphere. The lifetime of the state is assumed to be shortened by radiationless transitions to excited doublet states with smaller lifetimes. The energy difference between the fundamental and excited states is 7 kJ/mol.

The comparison between EPR spectra of $MFP^-$ in frozen solutions of MeTHF and THF, as well as between EPR and echo-detected EPR in THF, shows that the EPR line width in the latter case is due to an inhomogeneous broadening produced by radical clusters.

**Acknowledgment.** We thank Prof. C. Corvaja and U. Segre for helpful discussions, Mrs. E. Zangirolami for her technical support in the preparation of the radical anions, and Dr. Maria Luisa Martini for her help in the synthesis of the compounds. This work has been in part supported by the C.N.R. through its *Centro di Studio sugli Stati Molecolari Radicalici ed Eccitati*, Padova, and *Progetto Strategico Materiali Innovativi*.

## References and Notes

(1) Hase, H.; Miyatake, Y. *Chem. Phys. Lett.* **1995**, *245*, 95.
(2) Stasko, A.; Brezová, V.; Rapta, P.; Asmus, K. D.; Guldi, D. M. *Chem. Phys. Lett.* **1996**, *262*, 233.
(3) Iyoda, M.; Sasaki, S.; Yoshida, M.; Kuwatani, Y.; Nagase, S. *Tetrahedron Lett.* **1996**, *37*, 7987.
(4) Eaton, S. S.; Eaton, G. R. *Appl. Magn. Reson.* **1996**, *11*, 155.
(5) Baumgarten, M.; Ghergel, L. *Appl. Magn. Reson.* **1996**, *11*, 171.
(6) Rübsam, M.; Dinse, K. P.; Plüshau, M.; Fink, J.; Krätschmer, W.; Fostiropoulos, K.; Taliani, C. *J. Am. Chem. Soc.* **1992**, *114*, 10059.
(7) Boyd, P. D. W.; Bhyrappa, P.; Paul, P.; Stinchcombe, J.; Bolskar, R. D.; Stinchcombe, J. *J. Am. Chem. Soc.* **1995**, *117*, 2907.
(8) Dubois, D.; Jones, M. T.; Kadish, K. M. *J. Am. Chem. Soc.* **1992**, *114*, 6446.
(9) Allemand, P. M.; Srdanov, G.; Koch, A.; Khemani, K.; Wudl, F.; Rubin, Y.; Diederich, F.; Alvarez, M. M.; Anz, S. J.; Whetten, R. L. *J. Am. Chem. Soc.* **1991**, *113*, 2780.
(10) Stasko, A.; Brezová, V.; Biskupic, S.; Dinse, K. P.; Gross, R.; Baumgarten, M.; Gügel, A.; Belik, P. *J. Electroanal. Chem.* **1997**, *423*, 131.
(11) Stinchcombe, J.; Pénicaud, A.; Bhyrappa, P.; Boyd, P. D. W.; Reed, C. A. *J. Am. Chem. Soc.* **1993**, *115*, 5212.
(12) Maggini, M.; Scorrano, G.; Prato, M. *J. Am. Chem. Soc.* **1993**, *115*, 9798.
(13) Prato, M. *J. Mater. Chem.* **1997**, *7*, 1097.
(14) Imahori, H.; Sakata, Y. *Adv. Mater.* **1997**, *9*, 537.
(15) Sun, Y.; Drovetskaya, T.; Bolskar, R. D.; Bau, R.; Boyd, P. D. W.; Reed, C. A. *J. Org. Chem.* **1997**, *62*, 3642.
(16) Zoleo, A. Ph.D.Thesis, Padova, 1995.
(17) Maggini, M.; Scorrano, G.; Prato, M.; Brusatin, G.; Innocenzi, P.; Guglielmi, M.; Renier, A.; Signorini, R.; Meneghetti, M.; Bozio, R. *Adv. Mater.* **1995**, *7*, 404.
(18) Pasimeni, L.; Hirsh, A.; Lamparth, I.; Herzog, A.; Maggini, M.; Prato, M.; Corvaja, C.; Scorrano, G. *J. Am. Chem. Soc.* **1997**, *119*, 12896.
(19) Ramakrishnan, S.; Boulas, P.; Vijayashree, M. N.; D'Souza, F.; Jones, M. T.; Kadish, K. M. *J. Chem. Soc., Chem. Commun.* **1994**, 1847.
(20) Koga, N.; Morokuma, K. *Chem. Phys. Lett.* **1992**, *196*, 191.
(21) Arena, F.; Bullo, F.; Conti, F.; Corvaja, C.; Maggini, M.; Prato, M.; Scorrano, G. *J. Am. Chem. Soc.* **1997**, *119*, 789.
(22) Karplus, M.; Fränkel, G. K. *J. Chem. Phys.* **1961**, *35*, 1312.
(23) Atherton, N. M. *Principles of Electron Spin Resonance*; Ellis Horwood and Prentice Hall: New York, 1993.
(24) *Handbook of Chemistry and Physics*, 76th ed.; CRC Press: Boca Raton, FL, 1995−1996.
(25) Millhauser, G. L.; Freed, J. H. *J. Chem. Phys.* **1984**, 81, *37*.
(26) Kato, T.; Kodama, T.; Oyama, M.; Okazaki, S.; Shida, T.; Nakagawa, T.; Matsui, Y.; Suzuki, S.; Shiromaru, H.; Yamauchi, K.; Achiba, Y. *Chem. Phys. Lett.* **1991**, *186*, 35.
(27) Novais, H. M.; Steenken, S. *J. Am. Chem. Soc.* **1986**, *108*, 1.
(28) Pfafferot, G.; Oberhammer, H.; Boggs, J. E. *J. Am. Chem. Soc.* **1985**, *107*, 2309.
(29) Bagno, A.; Maggini, M.; Martini, M. L.; Prato, M.; Scorrano, G. Unpublished results.
(30) (a) Eiermann, M.; Haddon, C. R.; Knight, B.; Chan Li, Q.; Maggini, M.; Martin, N.; Ohno, T.; Prato, M.; Suzuki, T.; Wudl, F. *Angew. Chem., Int. Ed. Engl.* **1995**, *34*, 159. (b) Knight, B.; Martín, N.; Ohno, T.; Ortí, E.; Rovira, C.; Veciana, J. H.; Vidal-Ganced, J.; Viruela, P.; Viruela, R.; Wudl, F. *J. Am. Chem. Soc.* **1997**, *119*, 9871.
(31) Weil, J. A.; Bolton, J. R.; Wetz, J. E. *Electron Paramagnetic Resonance*; Wiley-Interscience: New York, 1994.
(32) Freed, J. H.; Kooser, R. G. *J. Chem. Phys.* **1968**, *49*, 4715.
(33) Shell-Sorokin, A. J.; Mehran, F.; Eaton, G. R.; Eaton, S. S.; Viehbeck, A.; O'Toole, T. R.; Brown, A. A. *Chem. Phys. Lett.* **1992**, *195*, 225.
(34) (a) Bezmelnitsin, V. N.; Eletskii, A. V.; Stepanov, E. V. *J. Phys. Chem.* **1994**, *98*, 6665. (b) Ying, Q.; Marecek, J.; Chu, B. *Chem. Phys. Lett.* **1994**, *219*, 214.